Journal of the Franklin Institute 361 (2024) 106839

Contents lists available at ScienceDirect

Journal of the Franklin Institute

journal homepage: www.elsevier.com/locate/fi

Integrated sensor FTC using integral sliding mode control

Lejun Chen [a], Christopher Edwards [b], Halim Alwi [b,*]

[a] College of Automation Engineering, Nanjing University of Aeronautics and Astronautics, China
[b] Department of Engineering, University of Exeter, UK

ARTICLE INFO

Keywords:
Sliding mode observers
Integral sliding mode
Fault tolerant control

ABSTRACT

In this paper, a sliding mode sensor fault tolerant control scheme which involves a first order sliding mode observer, fault compensation logic and an integral sliding mode controller, is proposed for a class of uncertain linear parameter-varying systems. The proposed scheme has the capability to retain near nominal fault-free performance in the face of a class of sensor faults/failures. In particular, the closed-loop stability of the sensor fault tolerant scheme involving the sliding mode observer and the sliding mode controller in the presence of faults and uncertainty, is rigorously analysed. Furthermore, the paper proposes an algorithm to simultaneously synthesize the design freedom associated with the observer gains and control law despite the lack of a separation principle in the closed loop system overall caused by the uncertainty. The proposed scheme is validated using a commercial aircraft model. Good simulation results show the efficacy of the scheme.

1. Introduction

One of the key properties of sliding mode observers (SMOs) is their capability to track measured plant outputs whilst simultaneously estimating exogenous signals (faults or disturbance) and the system states [1,2]. In a sensor fault scenario, if the corrupting faults can be accurately estimated (by the sliding mode observer), a 'virtual sensor' can be established, and the actual measured output corrected using the fault estimate [3]. Sensor fault tolerant control can then be induced if the virtual sensor is used as part of the feedback loop instead of the raw (corrupted) measurement. This approach has the advantage that it can help to retain close to nominal fault-free performance in a faulty situation without the necessity of reconfiguring the original baseline control law [4]. This can be very advantageous from a flight certification perspective. The approach is captured schematically in Fig. 1.

In Fig. 1, the sliding mode observer reconstructs the fault f, using only the known control inputs u_p and the measured outputs y_p. The fault reconstruction $\hat{f}$ then compensates the raw measurements before they are used in the feedback loop.

Integral sliding mode (ISM) control has been the subject of extensive research interest in recent years [5–10]. ISM based methodologies address the reaching phase problem in the face of matched uncertainties [11,12]. The ISM control law usually contains two components. One component is created to maintain the stability of the nominal plant and to introduce an appropriate level of performance, whilst the other discontinuous 'retro-fitted' component is included to induce a sliding motion and to compensate for the effect of matched uncertainty. Furthermore, an ISM controller allows the matched uncertainty to be compensated from the time control is initiated.

This paper proposes an active sensor fault tolerant control (FTC) scheme for a class of LPV systems involving a SMO and an ISM controller. In most conventional active sensor FTC schemes, the control law and the observer (representing the fault detection

* Corresponding author.
E-mail addresses: l.Chen@nuaa.edu.cn (L. Chen), c.edwards@exeter.ac.uk (C. Edwards), h.alwi@exeter.ac.uk (H. Alwi).

https://doi.org/10.1016/j.jfranklin.2024.106839
Received 12 May 2023; Received in revised form 25 December 2023; Accepted 11 April 2024
Available online 19 April 2024

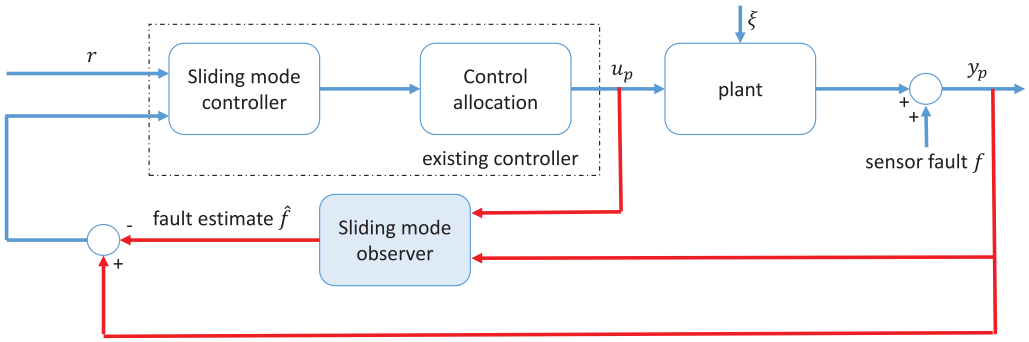

Fig. 1. The scheme of sensor FTC using SMO.

and isolation (FDI) aspect) are developed separately. This helps in terms of simplicity, but also has disadvantages. Also it is well understood that plant/model mismatches in the form of uncertainty introduces coupling between the controller and observer elements — and often affects the level of performance which can be achieved. Recently, more holistic integrated FDI and feedback control schemes have been proposed — see for example [13–15]. Broadly these approaches can be divided into two categories, depending on whether any FDI elements are explicitly included. In the works of [16–18], the fault signals in the residuals may be marginalized and dominated by the effects arising from external reference demands and the presence of uncertainty. This detrimentally affects the sensitivity of the residuals to the faults and can contribute to increased miss-detection rates. To counteract these disadvantages, higher order controllers need to be adopted to create the control and the residual signals. The integrated schemes [3,19–21], incorporate explicit observer and controller structures, and are of fixed order. Here the objective is to attempt to decouple the residual signals from the effects of the control laws. In this situation, the sensitivity of the residual to modelling uncertainty is crucial and necessitates the FDI component being highly robust with respect to the plant/model uncertainties.

The author's previous work in [22] integrated a conventional SMO and an SMC to ensure fault tolerance in the face of sensor faults. In contrast, the scheme proposed here is quite different from the one in [22]. Compared with [22], the proposed scheme described in this paper develops an integral siding surface involving the compensated states, and it ensures the sliding motion occurs from the beginning of the simulation. Furthermore in the literature, very few works attempt to formally analyse the stability of the FTC scheme which involves both a SMO and a SMC in the feedback loop. A rigorous stability analysis of the closed-loop FTC system involving an ISM controller is investigated in this paper. In addition, a locally optimal solution, selecting all the design parameters, can be synthesized using an iterative matrix inequality based approach (which was not discussed in [22]). In this sense, the work described in this paper is both rigorous and *constructive*. The algorithm which is proposed simultaneously synthesizes the design freedom associated with the observer gains and control law, despite the lack of a separation principle caused by the uncertainty.

The paper is organized as follows: in Section 2, the LPV SMO is described; whilst in Section 3, the ISM controller design is discussed and the closed-loop stability is analysed. Section 4 introduces an LPV/BMI problem which must be solved to simultaneously obtain the observer and controller gains. An iterative algorithm is then proposed to solve this problem. Finally, a commercial aircraft model case study is undertaken in Section 5 to demonstrate the efficiency of the scheme.

2. LPV sliding mode fault reconstruction

Consider the uncertain LPV system subject to sensor faults given by

$$\begin{aligned} \dot{x}_p(t) &= A_p(\rho)x_p(t) + B_p(\rho)u_p(t) + M_p(\rho)\xi(x_p,t) \\ y_p(t) &= x_p(t) + H_p f(t) \\ z_\infty(t) &= C_c x_p(t) \end{aligned} \tag{1}$$

where $A_p(\rho) \in \mathbb{R}^{n\times n}$, $B_p(\rho) \in \mathbb{R}^{n\times m}$, $M_p(\rho) \in \mathbb{R}^{n\times k}$ and $C_c \in \mathbb{R}^{h\times n}$. In Eq. (1), $x_p(t)$, $u_p(t)$ and $y_p(t)$ denote the system states, the control inputs and the measured outputs, respectively. The scheduling parameters $\rho \in \Omega \subset \mathbb{R}^{n_r}$ are assumed to be perfectly measurable and lie in a compact set Ω. The matrix $H_p \in \mathbb{R}^{n\times q}$ in Eq. (1) describes how the faults $f(t)$ corrupt the measurements. Here it is assumed that $\mathrm{rank}(H_p) = q$ where $q < n$, and that H_p is formed from columns belonging to the standard basis for $\mathbb{R}^n$. The signal $f(t)$ is assumed to be piecewise differentiable and represents the unknown sensor faults. Furthermore the fault signals are assumed to be bounded and satisfy $\|f(t)\| \le \bar{f}_{max}$ where $\bar{f}_{max}$ is a known positive constant. This value would be chosen a-priori based on a physical understanding of the sensors and their range, based on normal fault free behaviour.

The signal $z_\infty(t)$ encapsulates a measure of performance and is to be minimized [23]: specifically, as part of the design process, the gains in the observer and controller structure will be optimized to ensure

$$\int_0^\infty \|z_\infty(s)ds\| \le \gamma \int_0^\infty \|\xi(s)\|ds$$

where $\gamma > 0$ is small and ξ is the lumped disturbance present in (1).

In Eq. (1) is assumed that $\|\xi(\cdot)\| \leq c_1\|x_p(t)\| + c_2(t)$ where $c_1 > 0$ is a known constant and $c_2(t)$ is an unknown scalar function which satisfies $\|c_2(t)\| \leq d$ where d is a known constant.

Remark 2.1. In the representation in (1), each column of H_p is identified with a fault on a particular sensor, and as a consequence, up to $q < n$ faults are considered. The resulting FTC scheme aims to provide tolerance to faults within the subset of the measurements defined by H_p. The matrix H_p can be viewed as a design choice, and would be selected in an application specific way to address faults which would be considered as the most safety critical.

Since H_p is formed of columns from the standard basis for $\mathbb{R}^n$, the system outputs $y_p(t)$ can be permuted and then partitioned as

$$\begin{bmatrix} y_{p,1}(t) \\ y_{p,2}(t) \end{bmatrix} = \begin{bmatrix} C_1 \\ C_2 \end{bmatrix} x_p(t) + \begin{bmatrix} 0 \\ I_q \end{bmatrix} f(t) \tag{2}$$

where the $y_{p,1}(t)$ are fault free sensor measurements whilst the set $y_{p,2}(t)$ are corrupted by faults. In Eq. (2), $C_1 \in \mathbb{R}^{(n-q)\times n}$ is formed from rows of the identity matrix and satisfies $\mathrm{rank}(C_1) = n - q$ and $C_2 \in \mathbb{R}^{q\times n}$.

Assumption 2.1. The pair $(A_p(\rho), C_1)$ is quadratically detectable.

To formulate the sensor fault as an unknown input so that a classical SMO design scheme can be employed [2], a first order filter will be introduced defined as

$$\dot{z}_f(t) = -A_f z_f(t) + A_f y_{p,2}(t) \tag{3}$$

where $A_f \in \mathbb{R}^{q\times q}$ is a symmetric positive definite (s.p.d) matrix. Notice that a good choice of A_f can be used to help mitigate the degradation of the fault estimation performance in the presence of unmatched uncertainties [2].

Combine Eqs. (1) and (3) to create an augmented system, and then apply a coordinate transformation $\mathrm{col}(x_p, x_f) \mapsto x_a$ given by

$$x_a = \begin{bmatrix} T_s & 0 \\ 0 & I_q \end{bmatrix} \begin{bmatrix} x_p \\ z_f \end{bmatrix} \tag{4}$$

where $T_s \in \mathbb{R}^{n\times n}$ is a permutation matrix which satisfies $C_1 T_s^{-1} = \begin{bmatrix} 0 & I_{n-q} \end{bmatrix}$. The overall system in the new coordinates takes the form

$$\begin{aligned} \dot{x}_a(t) &= A(\rho)x_a(t) + B(\rho)u_p(t) + Df(t) + M(\rho)\xi(\cdot) \\ y(t) &= Cx_a(t) \end{aligned} \tag{5}$$

where $x_a \in \mathbb{R}^{n+q}$, $y = \mathrm{col}(y_{p,1}, z_f)$ and $D = [0 \;\; A_f]^T$. As a result of the coordinate transformation in (4), the system matrix in (5) is given by

$$A(\rho) = \begin{bmatrix} T_s & 0 \\ 0 & I_q \end{bmatrix} \begin{bmatrix} A_p(\rho) & 0 \\ A_f C_2 & -A_f \end{bmatrix} \begin{bmatrix} T_s^{-1} & 0 \\ 0 & I_q \end{bmatrix} = \begin{bmatrix} T_s A_p(\rho) T_s^{-1} & 0 \\ A_f C_2 T_s^{-1} & -A_f \end{bmatrix} \tag{6}$$

the output distribution matrix

$$C = \begin{bmatrix} C_1 & 0 \\ 0 & I_q \end{bmatrix} \begin{bmatrix} T_s^{-1} & 0 \\ 0 & I_q \end{bmatrix} = \left[\begin{array}{cc|c} 0 & I_{n-q} & 0 \\ 0 & 0 & I_q \end{array}\right] = \begin{bmatrix} 0 & I_n \end{bmatrix} \tag{7}$$

and

$$M(\rho) = \begin{bmatrix} T_s M_p(\rho) \\ 0 \end{bmatrix} \tag{8}$$

For the system in Eq. (5), an LPV sliding mode observer is proposed taking the form

$$\dot{z}(t) = A(\rho)z(t) + B(\rho)u_p(t) + G_l(\rho)e_y(t) + G_n\nu(t) \tag{9}$$

where

$$\nu = -k(t)\frac{e_y}{\|e_y\|} \qquad \text{if} \quad e_y \neq 0 \tag{10}$$

is a *discontinuous* output error injection vector used to induce sliding in the state estimation error subspace. In Eq. (10), the positive scalar $k(\cdot)$ is the modulation function to be determined and $e_y(t) = C(z(t) - x_a(t))$ represents the output estimation error.

To help with the exposition which follows, partition the augmented system and disturbance matrices in Eq. (5) as

$$A(\rho) := \begin{bmatrix} A_{11}(\rho) & A_{12}(\rho) \\ A_{21}(\rho) & A_{22}(\rho) \end{bmatrix}, \quad M(\rho) := \begin{bmatrix} M_1(\rho) \\ M_2(\rho) \end{bmatrix} \tag{11}$$

where $A_{11}(\rho) \in \mathbb{R}^{q\times q}$, $M_2(\rho) \in \mathbb{R}^{n\times k}$. From (6), since the bottom q rows of $A(\rho)$ do not depend on ρ, the sub-matrix $A_{21}(\rho)$ has the particular form

$$A_{21}(\rho) = \begin{bmatrix} A_{211}(\rho) \\ A_{212} \end{bmatrix} \tag{12}$$

where $A_{211}(\rho) \in \mathbb{R}^{(n-q)\times q}$ and $A_{212} \in \mathbb{R}^{q\times q}$. This structure is important to some of the analysis which follows.

In Eq. (9), the observer gains $G_l(\rho)$ and G_n are chosen to take the form

$$G_l(\rho) = \begin{bmatrix} A_{11}(\rho)L - A_{12}(\rho) + k_2 L \\ -A_{22}(\rho) + A_{21}(\rho)L - k_2 I \end{bmatrix}, \quad G_n = \begin{bmatrix} -L \\ I_n \end{bmatrix} \tag{13}$$

In Eq. (13) $L \in \mathbb{R}^{q\times n}$ has the particular structure

$$L = \begin{bmatrix} L_1 & 0 \end{bmatrix} \tag{14}$$

where $L_1 \in \mathbb{R}^{q\times(n-q)}$, and k_2 is a positive scalar. These two quantities represent the design freedom.

Remark 2.2. Since from Assumption 2.1, $(A_p(\rho), C_1)$ is quadratically detectable, the pair $(A_{11}(\rho), A_{211}(\rho))$ is also quadratically detectable. Hence there exists a s.p.d matrix P_1 and a gain L_1 such that

$$P_1(A_{11}(\rho) + L_1 A_{211}(\rho)) + (A_{11}(\rho) + L_1 A_{211}(\rho))^T P_1 < 0 \quad \forall\ \rho \in \Omega \tag{15}$$

Define

$$e = z - x_a = \mathrm{col}(e_1, e_y) \tag{16}$$

where $e_1 \in \mathbb{R}^q$, and define a coordinate transformation $\tilde{e} = T_L e$ where

$$T_L = \begin{bmatrix} I_q & L \\ 0 & I_n \end{bmatrix} \tag{17}$$

In the new coordinates, $\tilde{e} = \mathrm{col}(\tilde{e}_1, e_y)$ where $\tilde{e}_1 = e_1 + Le_y$. Because of the specific choice of $G_l(\rho)$ in (13), it is quite straightforward to show in the new coordinates

$$\dot{\tilde{e}}_1 = \tilde{A}_{11}(\rho)\tilde{e}_1 + \tilde{M}_1(\rho)\xi \tag{18}$$

$$\dot{e}_y = \tilde{A}_{21}(\rho)\tilde{e}_1 - k_2 e_y - v + \tilde{M}_2(\rho)\xi + D_2 f \tag{19}$$

where $\tilde{A}_{11}(\rho) = A_{11}(\rho) + LA_{21}(\rho)$, $\tilde{A}_{21}(\rho) = A_{21}(\rho)$; the disturbance distribution matrices $\tilde{M}_1(\rho) = M_1(\rho) + LM_2(\rho)$ and $\tilde{M}_2(\rho) = M_2(\rho)$; and $D_2 = \begin{bmatrix} 0 & A_f^T \end{bmatrix}^T$. Define the system matrix associated with the error system in (18)–(19) as

$$A_e(\rho) = \begin{bmatrix} \tilde{A}_{11}(\rho) & 0 \\ \tilde{A}_{21}(\rho) & -k_2 I_n \end{bmatrix} \tag{20}$$

and assume L is chosen so that Eq. (15) holds. Then as argued in [14], for any positive k_2, there exist s.d.p matrices Q_0 and

$$P = \mathrm{diag}(P_1, p_2 I_n) \tag{21}$$

(where the scalar $p_2 > 0$) such that

$$P\tilde{A}_e(\rho) + \tilde{A}_e(\rho)^T P + Q_0 < 0 \quad \forall \rho \in \Omega \tag{22}$$

Let $\eta_1(y_p, d)$ be any function, depending on the upper bound of the disturbance, with the property that

$$\|\xi\| \le c_1\|x_p\| + d \le \eta_1(y_p, d) \tag{23}$$

and define $q_0 := \frac{1}{2}\lambda_{min}(P^{-\frac{1}{2}} Q_0 P^{-\frac{1}{2}}) > 0$ where $\lambda_{min}(\cdot)$ denotes the minimum eigenvalue. Using these quantities define

$$\dot{\chi}(t) = -q_0\chi(t) + \|P^{\frac{1}{2}} T_L M(\rho)\|\eta_1(y_p, d), \quad \chi(0) = 0 \tag{24}$$

Let $V_e = \tilde{e}^T P\tilde{e}$ then using (18)–(19) together with (22), and assuming the modulation gain from (10) is chosen to satisfy $k(t) > \|D_2\|\|f\|$, then

$$\begin{aligned} \dot{V}_e &= -\tilde{e}^T Q_0 \tilde{e} - 2p_2 k(t)\|e_y\| + 2\tilde{e}^T P\tilde{M}(\rho)\xi + 2p_2 D_2 f \\ &= -\tilde{e}^T P^{1/2} P^{-1/2} Q_0 P^{-1/2} P^{1/2}\tilde{e} + 2\tilde{e}P^{1/2} P^{1/2}\tilde{M}(\rho)\xi \\ &\le -\lambda_{min}(P^{-1/2} Q_0 P^{1/2}) V_e + 2\sqrt{V_e}\|P^{1/2}\tilde{M}(\rho)\|\|\xi\| \\ &\le -\lambda_{min}(P^{-1/2} Q_0 P^{1/2}) V_e + 2\sqrt{V_e}\|P^{1/2}\tilde{M}(\rho)\|\eta_1(y_p, d) \end{aligned} \tag{25}$$

Define $\tilde{V} = \sqrt{V_e}$. Consequently $\dot{\tilde{V}} = \frac{1}{2}\dot{V}_e/\sqrt{V_e}$ and therefore from (25)

$$\dot{\tilde{V}}(t) \le -q_0\tilde{V} + \|P^{1/2}\tilde{M}(\rho)\|\eta_1(y_p, d) \tag{26}$$

Integrating both sides of (26) yields

$$\tilde{V}(t) \le e^{-q_0 t}\tilde{V}(0) + \int_0^t e^{-q_0(t-s)}\|P^{1/2}\tilde{M}(\rho)\|\eta_1(y_p, d) \tag{27}$$

Note in (27) the initial condition $\tilde{V}(0)$ is not known, but in finite time t_0 (say), since $q_0 > 0$,

$$e^{-q_0 t_0}\tilde{V}(0) \le \chi_0$$

for any positive (design) scalar χ_0. Thus for all $t > t_0$

$$\tilde{V}(t) \leq \chi_0 + \int_0^t e^{-q_0(t-s)} \| P^{1/2} \tilde{M}(\rho) \| \eta_1(y_p, d) ds$$

From solving (24), for all $t > t_0$,

$$\tilde{V}(t) \leq \chi(t) + \chi_0 \tag{28}$$

and since $\lambda_{min}(P)\|\tilde{e}(t)\|^2 < V_e(t)$, it follows

$$\|\tilde{e}(t)\| \leq \sqrt{V_e(t)/\lambda_{min}(P)} \leq (\chi(t) + \chi_0)/\sqrt{\lambda_{min}(P)}$$

exploiting inequality (28). Since $\|\tilde{e}_1(t)\| \leq \|\tilde{e}(t)\|$ it follows

$$\tilde{\chi}(t) := (\chi(t) + \chi_0)/\sqrt{\lambda_{min}(P)} \geq \|\tilde{e}_1(t)\| \tag{29}$$

for all $t \geq t_0 \geq 0$ for some (finite) time $t_0 > 0$. Let $a_{21}(t) = \|\tilde{A}_{21}(\rho)\|$ and $m_2(t) = \|\tilde{M}_2(\rho)\|$. Since $\tilde{\chi}(t)$ is known, the modulation function in Eq. (10) is selected as

$$k(t) = a_{21}(t)\tilde{\chi}(t) + \|D_2\| \bar{f}_{max} + m_2(t)\eta_1(y_p, d) + \eta \tag{30}$$

where η is a positive scalar. Note that since $\chi(t)$ is obtained from solving (24), the signal $\tilde{\chi}(t)$ is known in real time and therefore the RHS of (30) is known. Then, considering (19),

$$\begin{aligned} e_y^T \dot{e}_y &= e_y^T \tilde{A}_{21}(\rho)\tilde{e}_1 - k_2\|e_y\|^2 - k(t)\|e_y\| + e_y^T \tilde{M}_2(\rho)\xi + e_y^T D_2 f \\ &\leq \|e_y\|\|\tilde{A}_{21}(\rho)\|\|\tilde{e}_1\| - k(t)\|e_y\| + \|e_y\|\|\tilde{M}_2(\rho)\|\|\xi\| + \|e_y\|\|D_2\|\|f\| \end{aligned}$$

and thus choosing the modulation gain as in (30), guarantees $e_y^T \dot{e}_y \leq -\eta\|e_y\|$ and hence sliding occurs on

$$S_o = \{\tilde{e}(t) \in \mathbb{R}^{n+q} : C\tilde{e}(t) = e_y(t) = 0\} \tag{31}$$

in finite time.

Define a fault estimation signal according to

$$\hat{f} = W v_{eq} \tag{32}$$

where v_{eq} denotes the equivalent output error injection signal [24] and

$$W = \begin{bmatrix} 0 & A_f^{-1} \end{bmatrix} \tag{33}$$

where A_f is defined in Eq. (3). Note that by construction $W\tilde{M}_2(\rho) = 0$ and $WD_2 = I_q$, then from (19), during sliding

$$v_{eq} = \tilde{A}_{21}(\rho)\tilde{e}_1 - \tilde{M}_2(\rho)\xi + D_2 f \tag{34}$$

Therefore if the fault estimate error e_f is defined as $e_f = \hat{f} - f$, then from (19) and (34), during sliding, its evolution is governed by

$$\begin{aligned} \dot{\tilde{e}}_1 &= \tilde{A}_{11}(\rho)\tilde{e}_1 - \tilde{M}_1(\rho)\xi \\ e_f &= -A_f^{-1} A_{212}\tilde{e}_1 \end{aligned} \tag{35}$$

From Eq. (35), in the situation when $\xi = 0$, $\tilde{e}_1 \to 0$ asymptotically and therefore $e_f \to 0$ as $t \to \infty$. However when $\xi \neq 0$, e_f is non-vanishing and the gain L will be chosen, as part of the design process to ensure a given induced $\mathcal{L}_2$ norm for the system in Eq. (35).

3. Controller design and closed-loop analysis

In this paper, integrator states, depending on the controlled outputs

$$y_c(t) = C_c x_p(t) \tag{36}$$

where $C_c \in \mathbb{R}^{l \times n}$, will be employed to provide low frequency tracking behaviour in the controller. As shown in Fig. 1, to induce fault tolerance, the estimated fault is used to create a 'corrected' version of $x_p(t)$ in Eq. (36) given by

$$\hat{x}_p(t) = x_p(t) + H_p f(t) - H_p \hat{f}(t) = x_p(t) - H_p e_f(t) \tag{37}$$

Based on the above, the integral action states satisfy

$$\dot{x}_r(t) = r(t) - C_c \hat{x}_p(t) = r(t) - C_c x_p(t) + C_c H_p e_f(t) \tag{38}$$

where $r(t)$ is the reference signal which emerges from the pre-filter

$$\dot{r}(t) = \Gamma(r(t) - R_c) \tag{39}$$

In which R_c is fixed and $\Gamma \in \mathbb{R}^{l\times l}$ is Hurwitz. Define $x_c(t) = \mathrm{col}(x_r(t), x_p(t))$ then combining Eqs. (1) and (38) gives

$$\dot{x}_c(t) = A_c(\rho)x_c(t) + B_c(\rho)u_p(t) + B_r r(t) + M_c(\rho)\xi(\cdot) + H_c e_f(t) \tag{40}$$

where the system and input distribution matrices $A_c(\rho)$, $B_c(\rho)$, B_r, $M_c(\rho)$ take appropriate forms (see [25]), and in particular

$$H_c = \begin{bmatrix}(C_c H_p)^T & 0\end{bmatrix}^T \tag{41}$$

Based on this augmented form

$$z_\infty = \underbrace{\begin{bmatrix}0 & C_c\end{bmatrix}}_{C_\infty} x_c \tag{42}$$

where the performance signal z_∞ [23] is defined in Eq. (1). Here it is assumed the (augmented) input distribution matrix can be written as

$$B_c(\rho) = B_v B_2(\rho) \tag{43}$$

where $B_v \in \mathbb{R}^{(l+n)\times l}$ (and is of rank l), and the parameter dependent matrix $B_2(\rho) \in \mathbb{R}^{l\times m}$ has the property that $\mathrm{rank}(B_2(\rho)) = l$ for all $\rho \in \Omega$.

Remark 3.1. The decomposition in (43) is a common one in the literature concerning over-actuation and control allocation [26,27]. It is an assumption and is often referred to as the requirement for perfect factorization. The decomposition in Eq. (43) clearly implies that $rank(B_c) \leq rank(B_v)$ and in practice the factorization is chosen so that $rank(B_c) = rank(B_v)$. Since B_c has m columns (it is associated with m control inputs) whilst B_v has only l columns (where $l < m$), it equates with the system having redundancy and being over-actuated. This redundancy can then be exploited by control allocation to maintain performance in the event of total failures to certain actuators.

Without loss of generality (and by invoking a change of coordinates if necessary), it is assumed that

$$B_v = \begin{bmatrix}0\\ I_l\end{bmatrix} \tag{44}$$

For the developments which are to follow define

$$v(t) = B_2(\rho)u_p(t) \tag{45}$$

Using the definition of the virtual control in Eq. (45) the augmented system in Eq. (40) can be written as

$$\dot{x}_c(t) = A_c(\rho)x_c(t) + B_v v(t) + B_r r(t) + M_c(\rho)\xi(\cdot) + H_c e_f(t) \tag{46}$$

The virtual control will be designed using an ISM [9,28] approach. Let

$$G = (B_v^T B_v)^{-1} B_v^T \tag{47}$$

where B_v is from Eq. (44). Since by assumption, B_v has full column rank, the expression in Eq. (47) is well defined.

Define the ISM switching function as

$$\sigma(t) = G\hat{x}_c(t) + G\hat{x}_c(0) - \int_0^t G(A_c(\rho) - B_v F(\rho))\hat{x}_c(\tau)d\tau \tag{48}$$

where, as defined in Eq. (37), $\hat{x}_c$ is associated with the compensated measurements and the integral action states i.e. $\mathrm{col}(x_r, \hat{x}_p)$, and therefore satisfies

$$\hat{x}_c = x_c - \hat{H}_c e_f \tag{49}$$

where e_f is the error in the fault estimate and

$$\hat{H}_c = \begin{bmatrix}-C_c H_p\\ H_p\end{bmatrix} \tag{50}$$

In Eq. (48) the gain $F(\rho)$ is to be chosen to make $A(\rho) - B_v F(\rho)$ quadratically stable. By construction, $\hat{x}_c$ in Eq. (49) is known (although both x_c and e_f are not). Note that G defined in Eq. (47) has the property that

$$GB_r = 0 \quad \text{and} \quad GB_v = I_l \tag{51}$$

Differentiating Eq. (48) along the system trajectories, and using Eq. (40) and the properties in Eq. (51) results in

$$\begin{aligned}\dot{\sigma} &= GA_c(\rho)x_c + v + GM_c(\rho)\xi + GH_c e_f - GA_c(\rho)\hat{x}_c + F(\rho)\hat{x}_c - G\hat{H}_c\dot{e}_f\\ &= GA_c(\rho)\hat{x}_c + GA_c(\rho)\hat{H}_c e_f + v + GM_c(\rho)\xi + GH_c e_f - GA_c(\rho)\hat{x}_c + F(\rho)\hat{x}_c - G\hat{H}_c\dot{e}_f\\ &= v + F(\rho)\hat{x}_c + (GA_c(\rho)\hat{H}_c + GH_c)e_f + GM_c(\rho)\xi - G\hat{H}_c\dot{e}_f\end{aligned} \tag{52}$$

Let the virtual control take the form

$$\upsilon = -F(\rho)\hat{x}_c + \upsilon^n \tag{53}$$

where

$$\upsilon^n = -\mathcal{K}(t)\frac{\sigma}{\|\sigma\|} \tag{54}$$

and the modulation gain $\mathcal{K}(t)$ is to be defined. Then it follows from Eq. (52)

$$\dot{\sigma} = \upsilon^n + (GA_c(\rho)\hat{H}_c + GH_c)e_f + GM_c(\rho)\xi - G\hat{H}_c\dot{e}_f \tag{55}$$

The term υ^n will now be chosen to enforce a sliding motion on $\sigma \equiv 0$ by choice of the modulation gain $\mathcal{K}(t)$. Using Eq. (35), the term $\dot{e}_f$ will now be removed: specifically Eq. (55) can be written as

$$\dot{\sigma} = \upsilon^n + \left(G\hat{H}_cA_f^{-1}A_{212}\tilde{A}_{11}(\rho) - (GA_c(\rho)\hat{H}_c + GH_c)A_f^{-1}A_{212}\right)\tilde{e}_1 + \left(GM_c(\rho) - G\hat{H}_cA_f^{-1}A_{212}\tilde{M}_1(\rho)\right)\xi \tag{56}$$

Proposition 3.1. *If the modulation gain in Eq. (54) is chosen to satisfy*

$$\mathcal{K}(t) \geq \eta_0 + \|G\hat{H}_cA_f^{-1}A_{212}\tilde{A}_{11}(\rho) - (GA_c(\rho)\hat{H}_c + GH_c)A_f^{-1}A_{212}\|\tilde{\chi}(t) + \|GM_c(\rho) - G\hat{H}_cA_f^{-1}A_{212}\tilde{M}_1(\rho)\|\eta_1(y_p, d) \tag{57}$$

where $\tilde{\chi}(t)$ is defined in Eq. (29), $\eta_1(y_p, d)$ in Eq. (23) and $\eta_0 > 0$, then sliding takes place on $\sigma \equiv 0$ in finite time.

Proof. The output of the filter in Eq. (24) has the property that in finite time $\tilde{\chi}(t) \geq \|\tilde{e}_1(t)\|$. Also, by construction, $\eta_1(y_d, d)$ in Eq. (23) satisfies $\eta_1(y_d, d) \geq \|\xi\|$. Choose $V = \frac{1}{2}\sigma^T\sigma$, then

$$\begin{aligned}\dot{V} &= \sigma^T\upsilon^n + \left(G\hat{H}_cA_f^{-1}A_{212}\tilde{A}_{11}(\rho) - (GA_c(\rho)\hat{H}_c + GH_c)A_f^{-1}A_{212}\right)\tilde{e}_1 + \left(GM_c(\rho) - G\hat{H}_cA_f^{-1}A_{212}\tilde{M}_1(\rho)\right)\xi \\ &\leq \|\sigma\|\|G\hat{H}_cA_f^{-1}A_{212}\tilde{A}_{11}(\rho) - (GA_c(\rho)\hat{H}_c + GH_c)A_f^{-1}A_{212}\|\|\tilde{e}_1\| + \|\sigma\|\|GM_c(\rho) - G\hat{H}_cA_f^{-1}A_{212}\tilde{M}_1(\rho)\|\|\xi\| - \mathcal{K}(t)\|\sigma\|\end{aligned} \tag{58}$$

Since in finite time $\tilde{\chi}(t) \geq \|\tilde{e}_1(t)\|$ and $\eta_1(y_d, d) \geq \|\xi\|$, choosing $\mathcal{K}(t)$ to satisfy Eq. (57) implies in finite time

$$\dot{V} \leq -\eta_0\|\sigma\| = -\eta_0\sqrt{2}V^{\frac{1}{2}} \tag{59}$$

and so $V \equiv 0$ in finite time, and therefore $\sigma \equiv 0$ in finite time. □

Remark 3.2. Usually in an ISM setting sliding on $\sigma = 0$ can be ensured for all time because the surface has the property that $\sigma(0) = 0$. This property cannot be guaranteed here since the modulation gain can only be guaranteed to dominate the state estimation error after a finite amount of time because $\tilde{\chi}(t)$ only dominates $\|\tilde{e}_1(t)\|$ after a finite period of time.

During sliding, from Eq. (55), the equivalent injection signal necessary to maintain sliding is

$$\upsilon^n_{eq} = -(GA_c(\rho)\hat{H}_c + GH_c)e_f - GM_c(\rho)\xi + G\hat{H}_c\dot{e}_f \tag{60}$$

This expression will be used to analyse the sliding motion. Substituting $\upsilon_{eq} = -F(\rho)\hat{x}_c + \upsilon^n_{eq}$ into Eq. (46) yields

$$\begin{aligned}\dot{x}_c &= A_c(\rho)x_c - B_\upsilon F(\rho)\hat{x}_c - B_\upsilon(GA_c(\rho)\hat{H}_c + GH_c)e_f - B_\upsilon GM_c(\rho)\xi + B_\upsilon G\hat{H}_c\dot{e}_f + B_r r + M_c(\rho)\xi + H_c e_f \\ &= A_c(\rho)x_c - B_\upsilon F(\rho)x_c + B_\upsilon F(\rho)\hat{H}_c e_f - B_\upsilon(GA_c(\rho)\hat{H}_c + GH_c)e_f - B_\upsilon GM_c(\rho)\xi + B_\upsilon G\hat{H}_c\dot{e}_f + B_r r + M_c(\rho)\xi + H_c e_f \\ &= (A_c(\rho) - B_\upsilon F(\rho))x_c + B_\upsilon(F(\rho)\hat{H}_c - GA_c(\rho)\hat{H}_c - GH_c)e_f + H_c e_f + (I - B_\upsilon G)M_c(\rho)\xi + B_r r + B_\upsilon G\hat{H}_c\dot{e}_f\end{aligned} \tag{61}$$

Thus during sliding, the overall closed loop dynamics can be written as

$$\begin{aligned}\dot{x}_c &= (A_c(\rho) - B_v F(\rho))x_c - B_v F(\rho)\hat{H}_c A_f^{-1} A_{212}\tilde{e}_1 - H_c A_f^{-1} A_{212}\tilde{e}_1 - B_v\big(G\hat{H}_c A_f^{-1} A_{212}\tilde{A}_{11}(\rho) - (GA_c(\rho)\hat{H}_c + GH_c)A_f^{-1} A_{212}\big)\tilde{e}_1 \\ &\quad + \big((I - B_v G)M_c(\rho) + B_v G\hat{H}_c A_f^{-1} A_{212}\tilde{M}_1(\rho)\big)\xi + B_r r \\ \dot{\tilde{e}}_1 &= \tilde{A}_{11}(\rho)\tilde{e}_1 - \tilde{M}_1(\rho)\xi \end{aligned} \tag{62}$$

The two equations in (62) are coupled by the uncertainty ξ which depends on the state and satisfies the conic sector constraint $\|\xi\| < c_1\|x_c\| + c_2(t)$ since $x_c = \mathrm{col}(x_r, x_p)$. If $r = 0$ and $c_2(t) = 0$ then using the Small Gain Theorem the origin of the system in Eq. (62) is quadratically stable if the $\mathcal{L}_2$ gain of the mapping $\mathcal{H} : \xi \to x_c$ is less than $1/c_1$, where from Eq. (62) the operator

$$\mathcal{H} = \left[\begin{array}{cc|c} \begin{bmatrix} (A_c(\rho) - B_v F(\rho)) & -B_v F(\rho)\hat{H}_c A_f^{-1} A_{212} - H_{12}(\rho) \\ 0 & \tilde{A}_{11}(\rho) \end{bmatrix} & & \begin{bmatrix} M_h(\rho) \\ -\tilde{M}_1(\rho) \end{bmatrix} \\ \hline \begin{bmatrix} I & 0 \end{bmatrix} & & 0 \end{array}\right]$$

in which the term

$$H_{12}(\rho) = H_c A_f^{-1} A_{212} + B_v\big(-(GA_c(\rho)\hat{H}_c + GH_c)A_f^{-1} A_{212} + G\hat{H}_c A_f^{-1} A_{212}\tilde{A}_{11}(\rho)\big)$$

and

$$M_h(\rho) = (I - B_v G)M_c(\rho) + B_v G\hat{H}_c A_f^{-1} A_{212}\tilde{M}_1(\rho)$$

The operator $\mathcal{H}$ depends on the design freedom associated with the gains $F(\rho)$ and L_1. Separately, both $F(\rho)$ and L must as a minimum be chosen so that $A_c(\rho) - B_v F(\rho)$ and $\tilde{A}_{11}(\rho)$ are quadratically stable.

Suppose the design freedom G can be selected so that $G\hat{H}_c = 0$ (which is possible if the sensor faults belong to the null space $\mathcal{N}(B_v)$). In this case, the operator $\mathcal{H}$ simplifies somewhat to become

$$\hat{\mathcal{H}} : \left[\begin{array}{cc|c} \begin{bmatrix} (A_c(\rho) - B_v F(\rho)) & -B_v F(\rho)\hat{H}_c A_f^{-1} A_{212} - \hat{H}_{12}(\rho) \\ 0 & \tilde{A}_{11}(\rho) \end{bmatrix} & & \begin{bmatrix} \hat{M}_h(\rho) \\ -\tilde{M}_1(\rho) \end{bmatrix} \\ \hline \begin{bmatrix} I & 0 \end{bmatrix} & & 0 \end{array}\right] \tag{63}$$

where in this case the term $\hat{H}_{12}(\rho) = H_c A_f^{-1} A_{212} - B_v\big(GA_c(\rho)\hat{H}_c A_f^{-1} A_{212}\big)$ and $\hat{M}_h(\rho) = (I - B_v G)M_c(\rho)$.

Again if the induced $\mathcal{L}_2$ gain of the operator $\hat{\mathcal{H}}$ is less than $1/c_1$, the closed-loop system is guaranteed to be stable by the Small Gain Theorem. This slightly more simplified form of $\hat{\mathcal{H}}$ in (63) admits the possibility of introducing a BMI representation of the design problem.

The simultaneous design of the gains $F(\rho)$ and the observer parameter L associated with (63) will be discussed in the sequel.

4. Integrated synthesis of the controller/estimator

For the purposes of developing an iterative design algorithm, suppose the controller feedback gain in (48) is written as

$$F(\rho) = F_0(\rho) + \Delta(\rho) \tag{64}$$

where $F_0(\rho)$ is an initial choice of gain which has been computed independently (of the observer design) under the assumption that the system is fault free. A minimum design requirement is that $A_c(\rho) - B_v F_0(\rho)$ is stable. Any one of the methods discussed in [29] or [30] could be employed to guarantee that $A_c(\rho) - B_v F_0(\rho)$ is quadratically stable and the performance signal $z_\infty(t)$ remains small in the face of the uncertainty $\xi(\cdot)$. The problem may then be viewed as one of selecting the matrix $\Delta(\rho)$ to improve the performance of the closed-loop when sensor faults are present, taking into account the additional dynamics introduced by the observer used to estimate the fault.

To understand the effect of $\Delta(\rho)$ in Eq. (48), for design purposes, an error system is created according to

$$\dot{e}_z = (A_c(\rho) - B_v F_0(\rho))e_z - B_v\Delta(\rho)x_c \tag{65}$$

The motivation for Eq. (65) is that it represents the difference in state evolution between different two systems: one governed by the original system matrix $A_c(\rho) - B_v F_0(\rho)$ and the other governed by the system matrix $A_c(\rho) - B_v(F_0(\rho) + \Delta(\rho))$. The idea is that the performance of the first system governed by $A_c(\rho) - B_v F_0(\rho)$ represents the ideal closed loop performance, and therefore keeping e_z small should form part of the integrated design process.

Combining Eqs. (35), (63) and (65), the overall LPV system representing the dynamics between ξ and the overall performance measure defined as $w = \mathrm{col}(e_z, z_\infty, e_f)$ can be expressed as

$$\begin{aligned}
&\underbrace{\begin{bmatrix} \dot{e}_z \\ \dot{x}_c \\ \dot{\tilde{e}}_1 \end{bmatrix}}_{\dot{x}} = \underbrace{\begin{bmatrix} A_0(\rho) & -B_v\Delta(\rho) & 0 \\ 0 & A_0(\rho) - B_v\Delta(\rho) & -B_v(F_0(\rho)+\Delta(\rho))\hat{C}_0 - C_0 + B_vGA_c(\rho)\hat{C}_0 \\ 0 & 0 & A_{11}(\rho) + LA_{21}(\rho) \end{bmatrix}}_{A_a(\rho)} \underbrace{\begin{bmatrix} e_z \\ x_c \\ \tilde{e}_1 \end{bmatrix}}_{x} + \underbrace{\begin{bmatrix} 0 \\ (I - B_vG)M_c(\rho) \\ -(M_1(\rho) + LM_2(\rho)) \end{bmatrix}}_{M_a(\rho)} \xi \\
&\underbrace{\begin{bmatrix} e_z \\ z_\infty \\ e_f \end{bmatrix}}_{w} = \underbrace{\begin{bmatrix} I & 0 & 0 \\ 0 & C_\infty & 0 \\ 0 & 0 & -A_f^{-1}A_{212} \end{bmatrix}}_{C_a} \begin{bmatrix} e_z \\ x_c \\ \tilde{e}_1 \end{bmatrix}
\end{aligned} \tag{66}$$

where $A_0(\rho) = A_c(\rho) - B_vF_0(\rho)$, $C_0 = H_cA_f^{-1}A_{212}$ and $\hat{C}_0 = \hat{H}_cA_f^{-1}A_{212}$.

Define the matrix set

$$\mathcal{P} = \left\{ X \in \mathbb{S}^+_{2l+2n+q} \ : \ X = \mathrm{diag}(X_1, X_1, X_2),\ X_1 \in \mathbb{S}^+_{l+n},\ X_2 \in \mathbb{S}^+_q \right\} \tag{67}$$

then the design problem can be posed as: find the gain $\Delta(\rho)$ (and then from Eq. (64) the controller feedback gain $F(\rho)$), $P_a \in \mathcal{P}$ and an observer gain parameter L (simultaneously) to minimize γ, subject to

$$\Xi(P_a, A_a(\rho), M_a(\rho), C_a, \gamma) < 0 \quad \text{and} \quad P_a > 0 \tag{68}$$

where

$$\Xi(P_a, A_a(\rho), M_a(\rho), C_a, \gamma) := \begin{bmatrix} P_aA_a(\rho) + A_a(\rho)^TP_a & P_aM_a(\rho) & C_a^T \\ * & -\gamma I & 0 \\ * & * & -\gamma I \end{bmatrix} \tag{69}$$

and $A_a(\rho)$, $M_a(\rho)$ and C_a are defined in Eq. (66).

Remark 4.1. Satisfaction of the inequality in Eq. (68) constitutes a matrix inequality version of the Bounded Real Lemma and implies $\|w\|_2 \le \gamma\|\xi\|_2$. In the situation when $\|\xi\| < c_1\|x_p\|$, it follows $\|\xi\| < c_1\|x\|$ which x is defined in Eq. (66), and therefore if $\gamma \le 1/c_1$, the system in Eq. (62) is quadratically stable.

Remark 4.2. To reduce the design complexity, the set $\mathcal{P}$ in (67) has a specific structure. However, this imposes a certain level of conservatism in terms of estimating the $\mathcal{L}_2$ gain between w and ξ. Thus there exists a trade-off between simplicity of formulation and unacceptable conservatism (see for example [31]).

Since $A_a(\rho)$ in Eq. (66) depends on $\Delta(\rho)$, the inequality in Eq. (68) is bilinear and therefore the problem in Eq. (68) is non-convex. In this paper, a variation on the iterative approach proposed in [14] will be employed.

Assumption 4.1. It is assumed, all the system matrices $A_p(\rho)$, $F_0(\rho)$, $B_p(\rho)$ and $M_p(\rho)$ in Eq. (1) are affinely dependent on ρ. In particular

$$F_0(\rho) = \sum_{i=1}^{n_\rho} \zeta_i(\rho)F_{0i} \quad \Delta(\rho) = \sum_{i=1}^{n_\rho} \zeta_i(\rho)\Delta_i \tag{70}$$

where $\zeta_i(\rho) \ge 0$ and $\sum_{i=1}^{n_\rho} \zeta_i(\rho) = 1$.

Define another matrix set $\bar{\mathcal{P}} \subset \mathcal{P}$ as

$$\bar{\mathcal{P}} = \left\{ \bar{X} \in \mathbb{S}^+_{2l+2n+q} \ : \ \bar{X} = \mathrm{diag}(X_3, X_4, X_3, X_4, X_5),\ X_3 \in \mathbb{S}^+_n,\ X_4 \in \mathbb{S}^+_l,\ X_5 \in \mathbb{S}^+_q \right\} \tag{71}$$

The following lemma is crucial to what follows:

Lemma 4.1. *Suppose the decision variables $\Delta(\rho)$, L, γ and $P_a \in \mathcal{P}$ satisfy Eq. (68). Then there exists a change of coordinates $x \mapsto \bar{T}x = \bar{x}$ for the augmented system given in Eq. (66), where $\bar{T} = \mathrm{diag}(T, T, I_q)$ and the block diagonal matrix $T \in \mathbb{R}^{(n+l)\times(n+l)}$ is nonsingular, so that in the new coordinates $(A_a(\rho), M_a(\rho), C_a) \mapsto (\bar{A}_a(\rho), \bar{M}_a(\rho), \bar{C}_a)$ the corresponding Bounded Real Lemma inequality is given by*

$$\Xi(\bar{P}_a, \bar{A}_a(\rho), \bar{M}_a(\rho), \bar{C}_a, \gamma) < 0 \quad \text{and} \quad \bar{P}_a \in \bar{\mathcal{P}} \tag{72}$$

where $\bar{A}_a(\rho) = \bar{T}A_a(\rho)\bar{T}^{-1}$, $\bar{M}_a(\rho) = \bar{T}M_a(\rho)$, $\bar{C}_a = C_a\bar{T}^{-1}$. Furthermore, it is possible to choose T and hence $\bar{T}$ so that $\bar{P}_a = \mathrm{diag}(\bar{P}_1, \bar{P}_2, \bar{P}_1, \bar{P}_2, P_e)$ and $\bar{B}_v = TB_v = B_v$.

Proof. See [14]. □

Remark 4.3. Note that in Eq. (72)

$$\bar{P}_a\bar{A}_a(\rho) = \begin{bmatrix} \bar{P}\bar{A}_0(\rho) & -\bar{P}\bar{B}_v\Delta(\rho)C_cT^{-1} & 0 \\ 0 & \bar{P}\bar{A}_0(\rho) - \bar{P}\bar{B}_v\Delta(\rho)C_cT^{-1} & -\bar{P}\bar{B}_v(F_0(\rho) + \Delta(\rho) - GA_c(\rho))\hat{C}_0 - \bar{P}C_0 \\ 0 & 0 & P_e(A_{11} + LA_{21}) \end{bmatrix} \tag{73}$$

where $\bar{A}_0(\rho) = TA_0(\rho)T^{-1}$ and $\bar{P}$ takes the form

$$\bar{P} = \begin{bmatrix} \bar{P}_1 & 0 \\ 0 & \bar{P}_2 \end{bmatrix} \tag{74}$$

This block diagonal structure means

$$\bar{P}\bar{B}_v\Delta(\rho) = \begin{bmatrix} 0 \\ \bar{P}_2\Delta(\rho) \end{bmatrix} \tag{75}$$

Choosing $X(\rho) = \bar{P}_2\Delta(\rho)$ and $Y = P_eL$ makes the expression in Eq. 4.3 affine w.r.t $\bar{P}$, P_e, $X(\rho)$ and Y. This is crucial to what follows.

In order to set up the notation necessary to describe the algorithm, define

$$\begin{aligned} A_a(\rho)^{(j)} &= \begin{bmatrix} A_0(\rho) & -B_v(\sum_{i=1}^{j-1}\bar{\Delta}(\rho)^{(i)} + \bar{\Delta}(\rho)^{(j)})C_c & 0 \\ 0 & A_0(\rho) - B_v(\sum_{i=1}^{j-1}\bar{\Delta}(\rho)^{(i)} + \bar{\Delta}(\rho)^{(j)})C_c & -B_v(F_0(\rho) + \sum_{i=1}^{j-1}\bar{\Delta}(\rho)^{(i)} + \bar{\Delta}(\rho)^{(j)} - GA_c(\rho))\hat{C}_0 - C_0 \\ 0 & 0 & A_{11}(\rho) + L^{(j)}A_{21}(\rho) \end{bmatrix} \\ M_a(\rho)^{(j)} &= \begin{bmatrix} 0 \\ (I - B_vG)M_c(\rho) \\ -(M_1(\rho) + L^{(j)}M_2(\rho)) \end{bmatrix} \end{aligned} \tag{76}$$

Note that in (76), $\Delta(\rho)$ has been written as $\Delta(\rho) := \sum_{i=1}^{j-1}\bar{\Delta}(\rho)^{(i)} + \bar{\Delta}(\rho)^{(j)}$. Then the following iterative algorithm can be used to synthesize $\Delta(\rho)$ to create $F(\rho) = F_0(\rho) + \Delta(\rho)$.

Algorithm 3.1.

Step 0. Initialize $j = 1$ and select a suitable stopping criteria $\epsilon > 0$.

Step 1. Minimize γ w.r.t the variables $L^{(j)}$ and $P_a^{(j)} \in \mathcal{P}$, subject to the LMIs

$$\Xi(P_a^{(j)}, A_a(\rho)^{(j)}, M_a(\rho)^{(j)}, C_a, \gamma^{(j)}) < 0 \quad \text{and} \quad P_a^{(j)} > 0 \tag{77}$$

where $A_a(\rho)^{(j)}$ and $M_a(\rho)^{(j)}$ are defined in (76) and (76), and in the expression for $A_a(\rho)^{(j)}$, $\bar{\Delta}(\rho)^{(j)} = 0$. Since $P_a^{(j)} \in \mathcal{P}$ write $P_a^{(j)} = \mathrm{diag}(P^{(j)}, P^{(j)}, P_e^{(j)})$ where $P_e^{(j)} \in \mathbb{S}^+_{n-p+q}$. Then defining $Y = P_e^{(j)}L^{(j)}$, inequality Eq. (77) is affine w.r.t the variables $P^{(j)}$, $P_e^{(j)}$, Y and γ, and constitutes an LMI optimization problem. Let $\gamma^{(j)}$ represents the optimal value of γ obtained from the optimization process.

Step 2. Using the Lyapunov matrix $P^{(j)}$ from Step 1 and using the result of Lemma 4.1, create the change of coordinates matrix $\bar{T}^{(j)}$ exploiting the Lyapunov matrix $P_a^{(j)}$ from Step 1 and the fact that it belongs to $\mathcal{P}$.

Change coordinates, $(A_a(\rho)^{(j)}, C_a, M_a(\rho)^{(j)}) \mapsto (\bar{A}_a(\rho)^{(j)}, \bar{C}_a, \bar{M}_a(\rho)^{(j)})$ using $\bar{T}_{(j)}$. Then using the arguments used to prove Lemma 4.1 and the ideas discussed in Remark 4.3, the BRL inequality in the new coordinates becomes

$$\Xi(\bar{P}_a^{(j)}, \bar{A}_a(\rho)^{(j)}, \bar{M}_a(\rho)^{(j)}, \bar{C}_a, \bar{\gamma}) < 0 \quad \text{and} \quad \bar{P}_a^{(j)} > 0 \tag{78}$$

Note Eq. (78) has a feasible solution $\bar{P}^{(j)} = ((\bar{T}^{(j)})^{-1})^T P^{(j)}(\bar{T}^{(j)})^{-1} \in \bar{\mathcal{P}}$, $\bar{\Delta}(\rho)^{(j)} = 0$ and $\bar{\gamma} = \gamma^{(j)}$. Now minimize $\bar{\gamma}$ w.r.t the variable $L^{(j)}$, $\bar{\Delta}(\rho)^{(j)}$ where $\bar{P}_a^{(j)} \in \bar{\mathcal{P}}$ subject to Eq. (78).

Using the arguments in the proof of Lemma 4.1 if $\bar{P}_a^{(j)}$ is written as $\bar{P}_a^{(j)} = \mathrm{diag}(P_1^{(j)}, P_2^{(j)}, P_1^{(j)}, P_2^{(j)}, P_e^{(j)})$ and defining $X(\rho)^{(j)} = P_2^{(j)}\bar{\Delta}(\rho)^{(j)}$ and $Y = P_e^{(j)}L^{(j)}$ then Eq. (78) is affine w.r.t the decision variables $P_1^{(j)}$, $P_2^{(j)}$, $P_e^{(j)}$, $X(\rho)^{(j)}$ and Y. Let the optimal value of

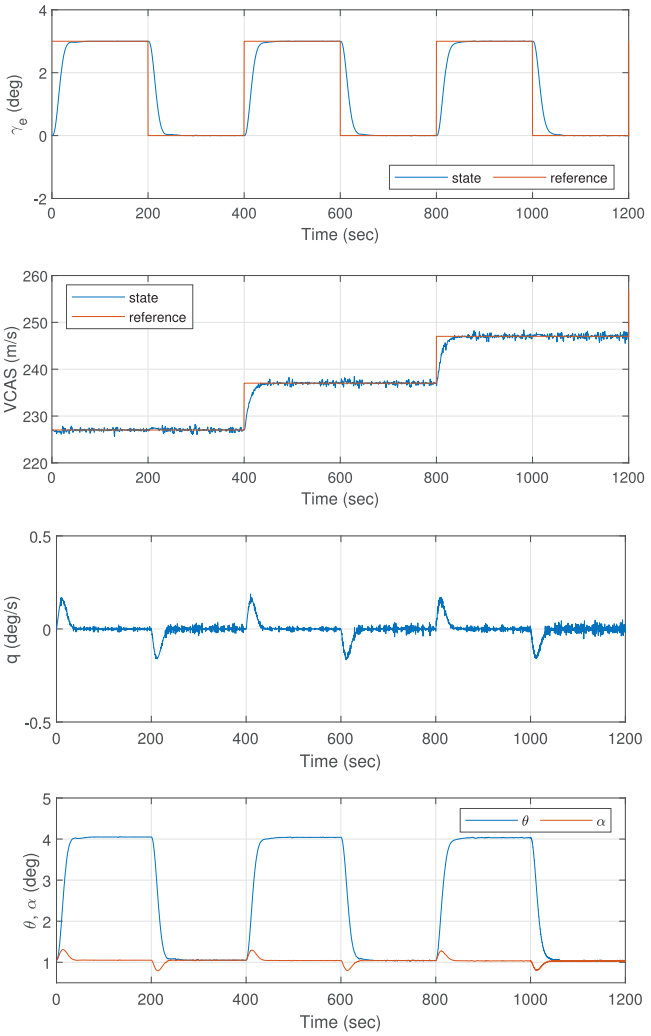

Fig. 2. Fault free: states.

$\bar{\gamma}$ in Eq. (78) be written $\bar{\gamma}^{(j)}$. Since Eq. (78) has a feasible solution in which $\bar{\Delta}(\rho)^{(j)} = 0$, the solution to the optimization guarantees $\bar{\gamma}^{(j)} \leq \gamma^{(j)}$.

Step 3. Define $\bar{\Delta}(\rho)^{(j)} = (P_2^{(j)})^{-1} B_u^{-1} X(\rho)^{(j)}$.

Step 4. If $|\bar{\gamma}^{(j)} - \gamma^{(j)}| < \epsilon$ then stop the iteration and a *local* optimal feasible solution for $F(\rho)$ and L is given by

$$F(\rho) = F_0(\rho) + \sum_{i=1}^{j} \bar{\Delta}(\rho)^{(i)} \quad L = L^{(j)} \tag{79}$$

Otherwise update the counter $j \to j+1$ and return to Step 1. □

During the current iteration, the component $\sum_{i=1}^{j-1} \bar{\Delta}(\rho)^{(i)}$, from earlier iterations, is treated as known. This component is aggregated with the initial value of the controller (i.e. $F_0(\rho) + \sum_{i=1}^{j-1} \bar{\Delta}(\rho)^{(i)}$) whilst $\bar{\Delta}(\rho)^{(j)}$ is treated as the decision variable in the current iteration. The algorithm guarantees the sequence of scalars $\gamma^{(j)}$ is always decreasing and is bounded from below by zero. Convergence of the algorithm in the sense that $\gamma^{(j)} \to \gamma^*$ as $j \to \infty$ is guaranteed and therefore the algorithm stopping criteria (Step 4) will always be satisfied.

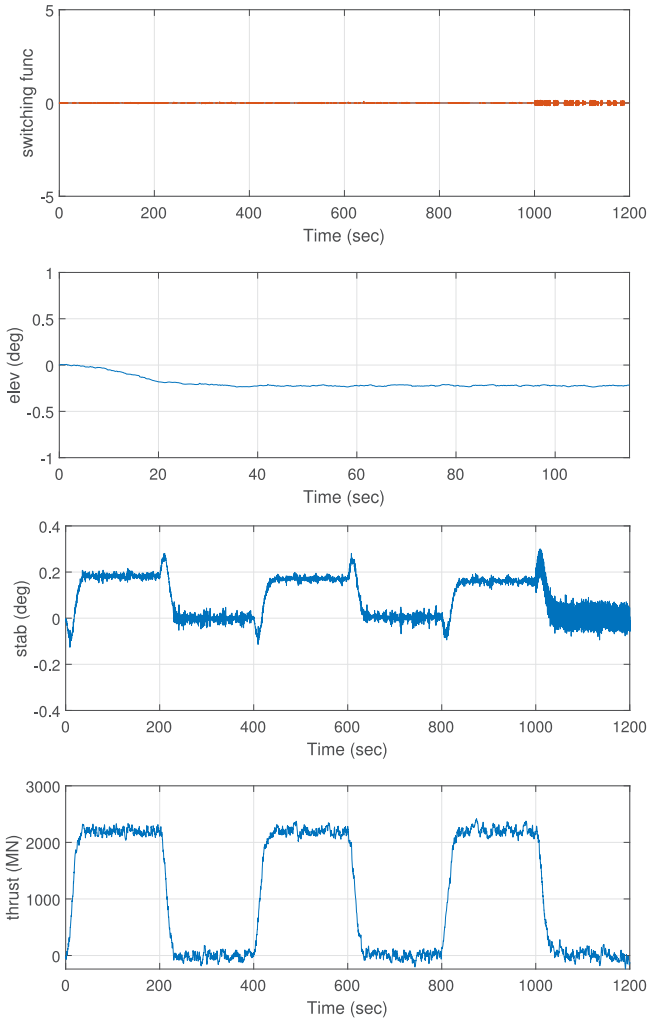

Fig. 3. Fault free: switching function σ and control inputs.

Remark 4.4. Since the optimization problem is non-convex, different initial choices of $F_0(\rho)$ potentially lead to different (locally optimal) solutions.

5. Design example

In this paper, the proposed scheme is tested using a longitudinal LPV commercial aircraft model [32,33]. The states of the LPV system are

$$x_p = \begin{bmatrix} \theta & \alpha & V_t & q \end{bmatrix} \tag{80}$$

which represents pitch angle, angle of attack, true airspeed and pitch rate, respectively. The system inputs are the elevator deflection, the stabilizer deflection and the engine thrust which are given by

$$u_p = \begin{bmatrix} \delta_e & \delta_s & T_n \end{bmatrix} \tag{81}$$

It is assumed that the controlled outputs are

$$y_c = \begin{bmatrix} \gamma_e & V_t \end{bmatrix} \tag{82}$$

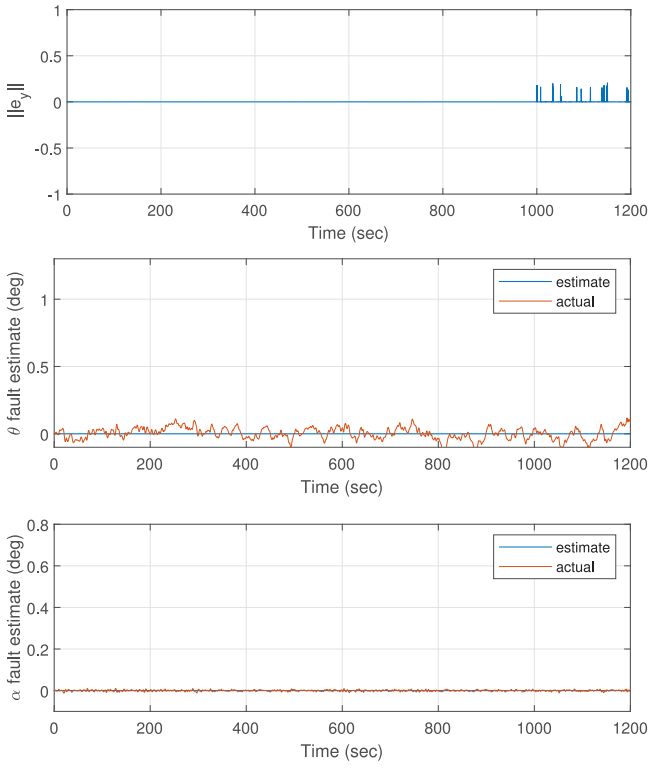

Fig. 4. Fault free: sliding surface $\|e_y\|$ and fault estimate.

where γ_e represents the flight path angle (FPA) and therefore the controlled-outputs distribution matrix C_c in Eq. (36) is

$$C_c = \begin{bmatrix} 1 & -1 & 0 & 0 \\ 0 & 0 & 1 & 0 \end{bmatrix} \tag{83}$$

At an altitude of 7000 m, the LPV model is obtained from the trim conditions

$$\begin{aligned} \begin{bmatrix} \theta_{trim} & \alpha_{trim} & V_{t,trim} & q_{trim} \end{bmatrix} &= \begin{bmatrix} 1.05 \text{ deg} & 1.05 \text{ deg} & 227.02 \text{ m/s} & 0 \text{ deg/s} \end{bmatrix} \\ \begin{bmatrix} \delta_{e,trim} & \delta_{s,trim} & T_{n,trim} \end{bmatrix} &= \begin{bmatrix} 0.163 \text{ deg} & 0.590 \text{ deg} & 42291 \text{ N} \end{bmatrix} \end{aligned} \tag{84}$$

The matrices $A_p(\rho)$ and $B_p(\rho)$ are assumed to depend affinely on the scheduling parameter ρ

$$A_p(\rho) = A_{p,0} + \sum_{i=1}^{4} A_{p,i} \quad \text{and} \quad B_p(\rho) = B_{p,0} + \sum_{i=1}^{4} B_{p,i} \tag{85}$$

where

$$\rho = \begin{bmatrix} \delta V_t & \delta V_t^2 & \delta V_t^3 & \delta V_t^4 \end{bmatrix} \tag{86}$$

and δV_t represents a perturbation in true airspeed from the trim value in (84). This representation is valid in the range $\delta V_t \in [-77.02\ 22.98]$ m/s [33]. The numerical values of $A_p(\rho)$ and $B_p(\rho)$ are taken from [32,33]. In this example, the matrix

$$B_v = \begin{bmatrix} 0_{4\times 2} \\ I_2 \end{bmatrix} \tag{87}$$

and the gain associated with the integral surface G, defined in Eq. (47), is chosen as

$$G = \begin{bmatrix} 0 & 0 & 0 & 0 & 1 & 0 \\ 0 & 0 & 0 & 0 & 0 & 1 \end{bmatrix} \tag{88}$$

The external disturbances considered in this paper arise from light forward turbulence and pitch rate turbulence at 7000 m generated using the Dryden Wind Turbulence model from the MATLAB Aerospace Toolbox. To demonstrate the robustness of the proposed

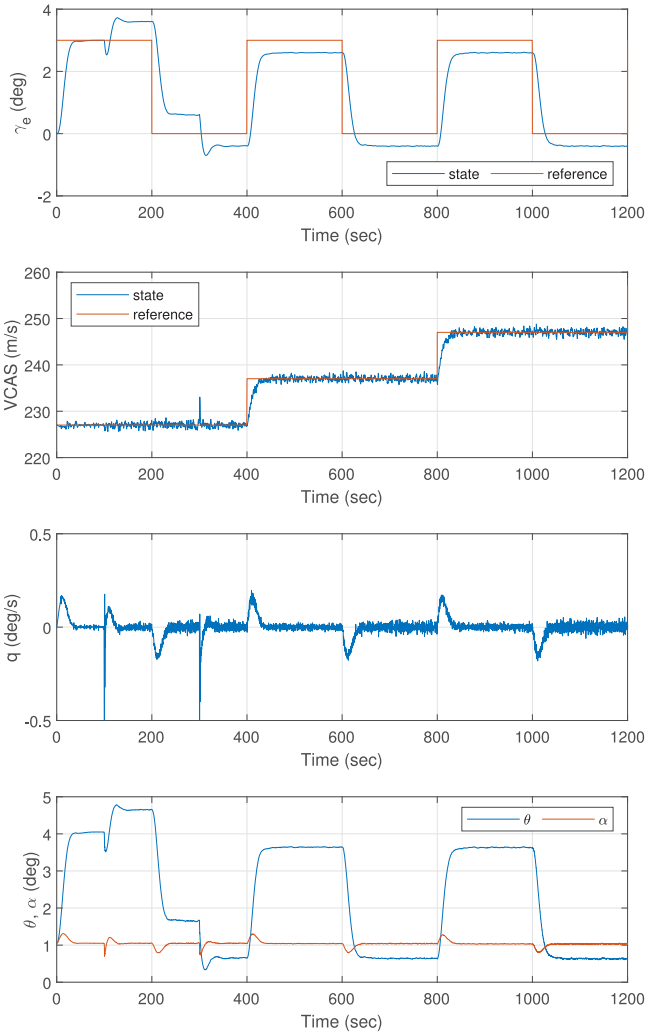

Fig. 5. Faulty case (with disturbance): states.

scheme in the face of measurement noise, it is assumed that Lebesgue measurable noise modelled as $0.003\sin(50t)$ occurs in the angle of attack, pitch angle and pitch rate measurements, and noise represented by $0.009\sin(50t)$ is injected into the velocity measurement. The noise is set to occur from 1000 s onwards in the simulations so that there is a noise-free portion to compare with. It is also assumed that the disturbances affect the V_t and q channels and therefore the disturbance distribution matrix

$$M_p(\rho) = \begin{bmatrix} 0 & 0 \\ 0 & 0 \\ 0 & 1 \\ 1 & 0 \end{bmatrix} \tag{89}$$

In terms of the observer design, the filter parameter in Eq. (9) is chosen as $A_f = 0.01 I_2$ and the scalar k_2 in Eq. (13) used to construct $G_l(\rho)$ was selected as $k_2 = 0.1$. In Eq. (10), the modulation gain $k(t)$ has been very conservatively chosen to be 1. To avoid chattering, the discontinuous unit vector term has been replaced by a sigmoidal approximation and the smoothing factor was chosen to be 0.01.

The nominal controller $F_0(\rho)$ was calculated to optimize the standard infinite horizon quadratic cost

$$J = \int_0^\infty x^T Q x + u^T R u \tag{90}$$

based on the nominal system represented by the pair $(A(\rho), B_v)$.

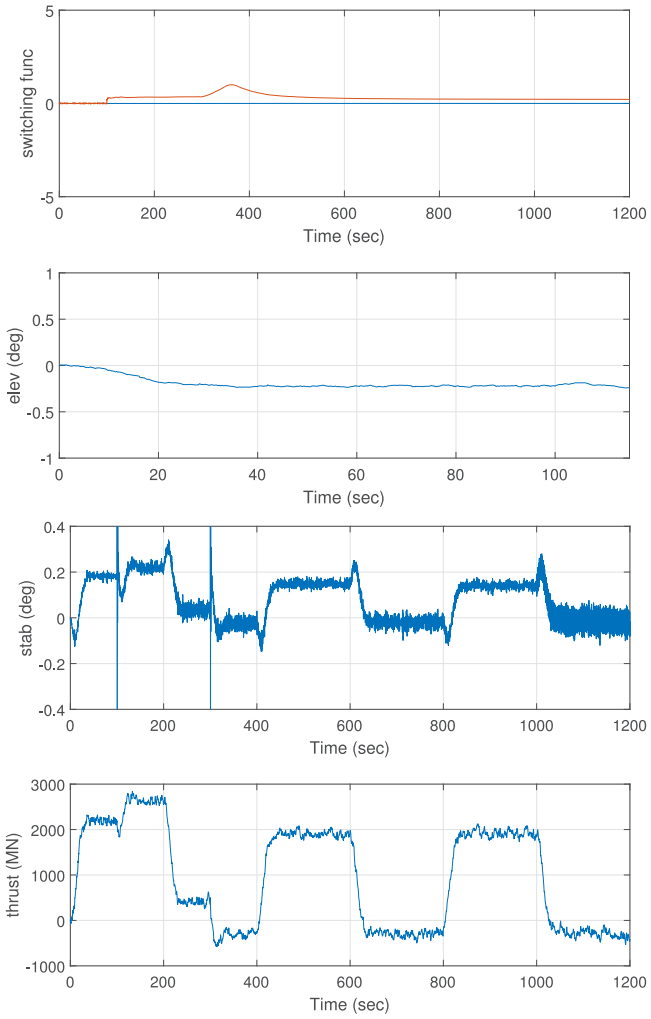

Fig. 6. Faulty case (with disturbance): control inputs.

Here Q and R are chosen as

$$Q = \text{diag}(1.1\ 0.05\ 1\ 1\ 0.03\ 5) \quad \text{and} \quad R = \text{diag}(0.007\ 1.1) \tag{91}$$

By solving the semidefinite programming problem:

$$\begin{aligned} &\min_{Y,Z,K(\rho)} \ \text{trace}(Z) \text{ subject to} \\ &\begin{bmatrix} -(A(\rho)Y - B_v K(\rho))^T - (A(\rho)Y - B_v K(\rho)) & Y & K^T(\rho) \\ Y & Q^{-1} & 0 \\ K^T(\rho) & 0 & R^{-1} \end{bmatrix} > 0 \\ &\begin{bmatrix} Z & I \\ I & Y \end{bmatrix} > 0 \end{aligned} \tag{92}$$

where Y is a s.p.d matrix and $K(\rho) = K_0 + \sum_{i=1}^{4} K_i \rho_i$. Then the nominal controller $F_0(\rho)$ can be obtained from

$$F_0(\rho) = K(\rho)Y^{-1} \tag{93}$$

The inequalities in arise from the use of the Schur complement, and constitute a well known LMI representation of the LQR-like problem associated with mimimizing (90).

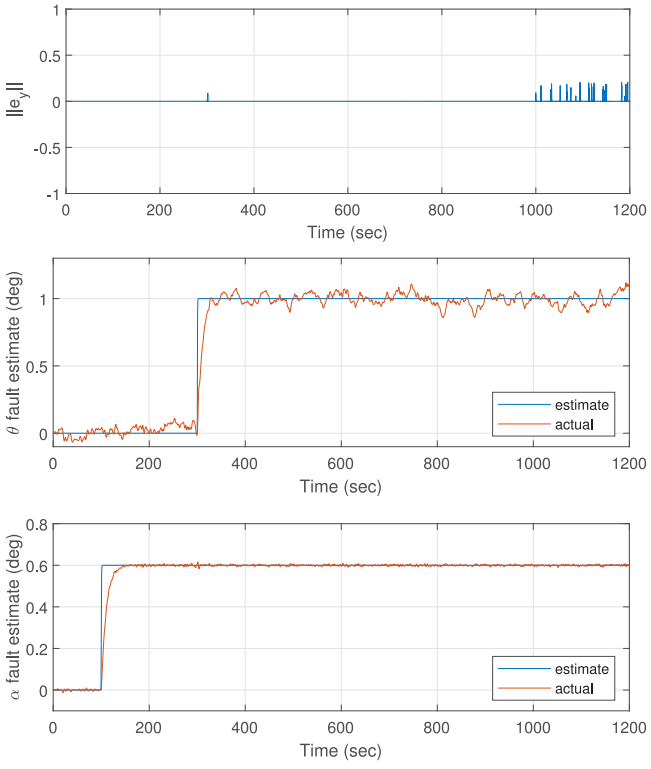

Fig. 7. Faulty case (with disturbance): sliding surface $\|e_y\|$ and fault estimate.

Using YALMIP with the SEDUMI LMI solver,[1] the values of Y and the nominal controller $F_0(\rho) = F_0 + \sum_{i=1}^{4} F_i \rho_i$ components are given by

$$Y = \begin{bmatrix} 98.1330 & -0.1129 & 13.2241 & 0.4038 & -0.0485 & 0.4431 \\ -0.1129 & 99.4635 & 0.6802 & 0.0465 & 0.5263 & -0.0323 \\ 13.2241 & 0.6802 & 6.2060 & 0.2865 & 0.4449 & -3.1034 \\ 0.4038 & 0.0465 & 0.2865 & 2.3122 & 0.5426 & -1.6072 \\ -0.0485 & 0.5263 & 0.4449 & 0.5426 & 99.4669 & 0.0792 \\ 0.4431 & -0.0323 & -3.1034 & -1.6072 & 0.0792 & 99.8647 \end{bmatrix} \tag{94}$$

$$\begin{aligned} F_0 &= \begin{bmatrix} -0.0186 & -1.0302 & -7.1129 & 7.8872 & 0.9839 & -0.0740 \\ -2.9282 & -0.1363 & 20.2474 & 37.1070 & -0.5462 & 2.0307 \end{bmatrix} \\ F_1 &= \begin{bmatrix} -0.0005 & -0.0001 & 0.0076 & -0.0222 & 0.0004 & 0.0041 \\ 0.0039 & -0.0006 & 0.0597 & -0.2627 & 0.0007 & 0.0330 \end{bmatrix} \\ F_2 &= \begin{bmatrix} -0.0000 & -0.0000 & 0.0001 & -0.0000 & -0.0003 & 0.0004 \\ -0.0023 & -0.0000 & 0.0004 & 0.0011 & -0.0048 & -0.0012 \end{bmatrix} \\ F_3 &= \begin{bmatrix} -0.0019 & 0.0000 & 0.0046 & 0.0090 & -0.0005 & 0.0139 \\ 0.0170 & 0.0005 & -0.0054 & -0.2585 & 0.0172 & 0.1432 \end{bmatrix} \times 10^{-8} \\ F_4 &= \begin{bmatrix} -0.0017 & -0.0000 & 0.0025 & 0.0178 & -0.0018 & -0.0015 \\ -0.0251 & -0.0003 & 0.0285 & 0.2581 & -0.0246 & -0.0300 \end{bmatrix} \times 10^{-9} \end{aligned} \tag{95}$$

The modulation gain in Eq. (54) was selected (conservatively) as $\mathcal{K}(t) = 0.4$. Using Algorithm 3.1, gives $\gamma = 4.0201$ and

$$L = \begin{bmatrix} -0.0875 & -2.6922 & 0 & 0 \\ 0.0520 & 0.5139 & 0 & 0 \end{bmatrix} \tag{96}$$

[1] https://yalmip.github.io/solver/sedumi/

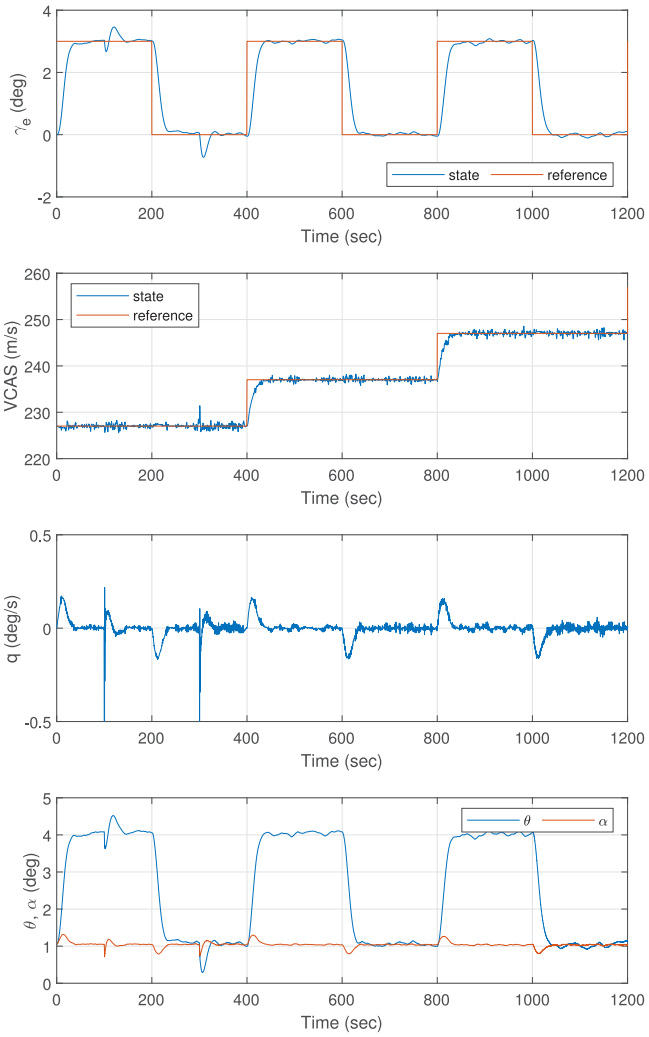

Fig. 8. Fault tolerance (with disturbance): states.

$$
\begin{aligned}
\Delta_0 &= \begin{bmatrix} -0.0401 & -0.0979 & -0.8432 & -1.8866 & 0.2764 & 0.6612 \\ -0.5315 & -0.1692 & 10.0344 & -0.3063 & -0.7166 & 8.1402 \end{bmatrix} \\
\Delta_1 &= \begin{bmatrix} 0.0097 & -0.0045 & -0.1455 & -0.2711 & 0.1486 & 0.0602 \\ 0.1530 & 0.0189 & -1.3575 & -3.9835 & -0.3026 & 1.2893 \end{bmatrix} \\
\Delta_2 &= \begin{bmatrix} -0.0000 & -0.0001 & 0.0006 & -0.0006 & 0.0004 & 0.0010 \\ -0.0001 & -0.0004 & -0.0000 & -0.0000 & 0.0012 & -0.0013 \end{bmatrix} \\
\Delta_3 &= \begin{bmatrix} -0.0023 & -0.0011 & 0.0537 & 0.0028 & -0.0064 & 0.0414 \\ 0.0269 & 0.0068 & -0.6801 & -0.0287 & 0.2697 & -0.4985 \end{bmatrix} \times 10^{-5} \\
\Delta_4 &= \begin{bmatrix} 0.0012 & 0.0044 & 0.0265 & -0.0016 & -0.0672 & 0.0082 \\ 0.0430 & 0.0117 & -0.2917 & -0.0362 & 0.0067 & -0.2241 \end{bmatrix} \times 10^{-6}
\end{aligned}
\tag{97}
$$

5.1. Simulation results

5.1.1. Fault free

In this section, fault free simulation results in the presence of external disturbances (wind/gusts) and sensor noise will be shown for the purpose of comparison. During the simulation, a series of 3deg FPA and 10 m/s true airspeed manoeuvres are created as the reference commands. Fig. 2 shows the aircraft states in the fault free situation. It can be seen from Fig. 2 that the ISM controller

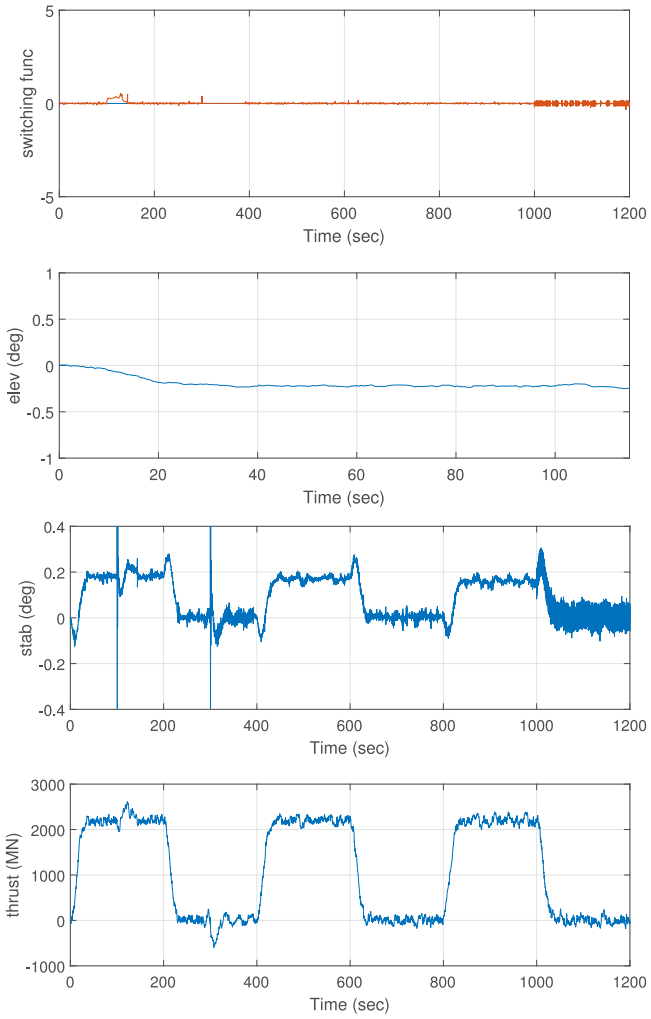

Fig. 9. Fault tolerance (with disturbance): switching function σ and control inputs.

has the capability to force the aircraft states to track the reference commands despite external disturbances and sensor noise. The trajectories of the aircraft states θ, α and q are shown in Fig. 2. The switching function associated with the ISM controller and the three control inputs generated from the ISM controller are shown in Fig. 3. In terms of observer performance, the sliding surface and the fault reconstruction signal are shown in Fig. 4. Clearly, in the absence of sensor faults, the fault estimate signal is close to zero (as it should be). In the simulation results, the effect of sensor noise can be seen from 1000 s onwards, especially in Fig. 3. Note that the paper is not concerned about fault detection and isolation per se and is focussed more on sensor fault tolerant control. However, from Fig. 4, it is clear a threshold can be selected around the reconstruction signals to provide detection and isolation of sensor faults. (Although this information is not needed in this paper).

5.1.2. Simultaneous pitch and angle of attack sensor faults — without sensor fault tolerant

In the faulty case, both the pitch and angle of attack sensors are assumed to be corrupted by sensor bias (to represent a sensor fault). The bias associated with the pitch angle measurements is set to be 1 deg and occurs at 300 s. The angle of attack sensor bias is set to be 0.6 deg and is assumed to occur from 100 s onwards. The external disturbances resulting from wind turbulence, occur throughout the simulation and as before, the sensor noise occurs from 1000 s onwards. The trajectories of the aircraft states in the faulty case (without FTC) are shown in Figs. 5–7. In this test, the fault estimates are not used to correct the measurements of pitch angle and angle of attack. Unsurprisingly, as can be seen from Figs. 5, the FPA tracking performance is degraded in the face of simultaneous angle of attack and pitch angle biases. This can be seen at 100 and 300 s when the sensor faults occur, and subsequently, a visible degradation in tracking performance can be seen in the flight path angle tracking. Fig. 7 shows good fault reconstruction for both the pitch and angle of attack sensors. Note that although not implemented (and not the focus of the paper), the fault reconstruction figure shows that the faults could be detected and isolated relatively quickly if carefully selected thresholds

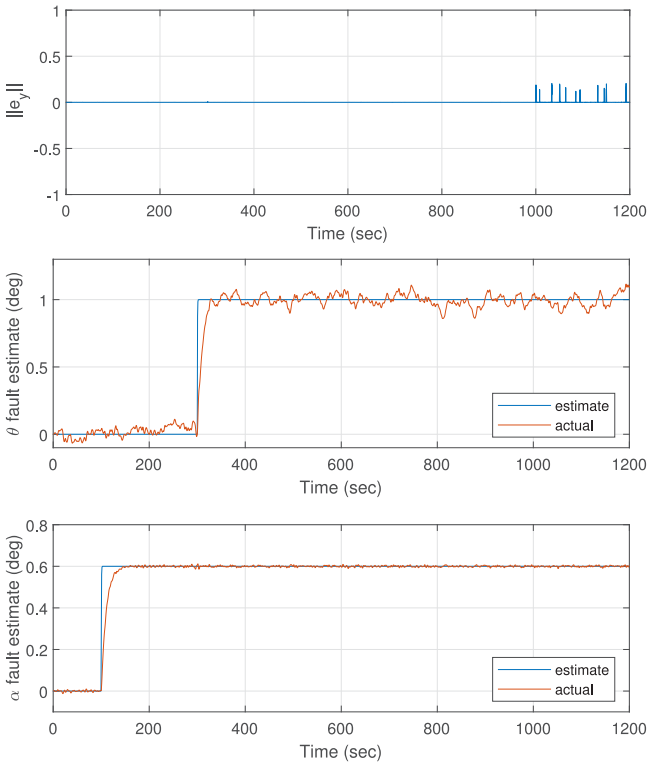

Fig. 10. Fault tolerance (with disturbance): sliding surface $\|e_y\|$ and fault estimate.

are chosen around zero in the reconstruction signals. Fig. 7 also shows the switching function of the observer is close to zero indicating good sliding performance. Fig. 6 shows the control surface deflections and the controller switching function. Again the effect of sensor noise can be seen in this figure, especially on the stabilizer signals after 1000 s

5.1.3. Simultaneous pitch and angle of attack sensor faults — without sensor fault tolerant

Figs. 8–10 show the fault tolerant performance of the proposed scheme in the presence of the angle of attack and pitch angle sensor faults (with wind/turbulence and sensor noise). The trajectories of the aircraft states in the face of the sensor bias and wind turbulence are shown in Fig. 8 where it can be seen that the aircraft states are still capable of following the reference commands. At 100 and 300 s, a small deviation can be seen from the flight path angle tracking, until the fault reconstruction estimates the correct fault level. The small deviation shows the effect of the filter (required to minimize the effect of noise and wind/gust) when extracting the equivalent output error injection. However, this discrepancy quickly disappears and tracking performance is regained. Fig. 9 displays the switching function of the ISM controller (and shows pseudo-sliding is maintained) and the control inputs generated from the ISM controller. From Fig. 10, both the pitch angle and angle of attack sensor faults can be seen to be well estimated and the sliding surface is close to zero. As before, the effect of sensor noise can be seen after 1000 s, especially on the control signals in Fig. 9. The simulation results show that the FTC performance is still retained despite sensor noise.

6. Conclusion

In this paper, a linear parameter varying integral sliding mode sensor FTC scheme has been proposed in which a sliding mode observer is employed to create sensor fault estimates to compensate the effect of corrupted sensor readings. This approach addresses the problem of the robustness of the sensor faults/failures reconstruction process, and the closed-loop reference tracking performance in the presence of external disturbances. It is shown that the scheme retains near to nominal closed-loop performance in the face of sensor faults/failures. Furthermore, a rigorous analysis of the closed-loop stability of the sensor fault tolerant scheme involving the sliding mode observer and the sliding mode controller is given. Importantly an algorithm is proposed to simultaneously synthesize the gains associated with the controller and the observer. This adds to the practicality of the scheme. The FTC scheme has been tested using an LPV commercial aircraft model. Good simulation results show the efficacy of the proposed scheme.

Declaration of competing interest

The authors declare that they have no known competing financial interests or personal relationships that could have appeared to influence the work reported in this paper.

Acknowledgement

This origin of this work was supported by the EU H2020 under grant agreement No. 690811 and the Japan NEDO under grant agreement No. 062800, as a part of the VISION project.

References

[1] C. Edwards, S.K. Spurgeon, Sliding Mode Control: Theory and Applications, Taylor & Francis, 1998.
[2] H. Alwi, C. Edwards, C.P. Tan, Fault Detection and Fault-Tolerant Control Using Sliding Modes, Springer, London, 2011.
[3] H. Alwi, C. Edwards, Fault detection and fault-tolerant control of a civil aircraft using a sliding-mode-based scheme, IEEE Trans. Control Syst. Technol. 16 (3) (2008) 499–510.
[4] H. Alwi, C. Edwards, Development and application of sliding mode LPV fault reconstruction schemes for the ADDSAFE benchmark, Control Eng. Pract. 31 (2014) 148–170.
[5] M. Basin, J. Rodriguez-Gonzalez, L. Fridman, Optimal and robust control for linear state-delay systems, J. Franklin Inst. 344 (6) (2007) 830–845.
[6] W.J. Cao, J.X. Xu, Nonlinear integral-type sliding surface for both matched and unmatched uncertain systems, IEEE Trans. Automat. Control 49 (8) (2004) 1355–1360.
[7] M. Rubagotti, A. Estrada, F. Castanos, A. Ferrara, L. Fridman, Integral sliding mode control for nonlinear systems with matched and unmatched perturbations, IEEE Trans. Automat. Control 56 (11) (2011) 2699–2704.
[8] H. Alwi, C. Edwards, Fault Tolerant Longitudinal Aircraft Control Using Non-Linear Integral Sliding Mode, IET Control Theory Appl, 2014.
[9] M.T. Hamayun, C. Edwards, H. Alwi, Fault Tolerant Control Schemes Using Integral Sliding Modes, Cham, Springer, 2016.
[10] L. Chen, H. Alwi, C. Edwards, Development and evaluation of an integral sliding mode fault-tolerant control scheme on the RECONFIGURE benchmark, Internat. J. Robust Nonlinear Control 29 (16) (2017) 5314–5340.
[11] G.P. Matthews, R.A. DeCarlo, Decentralized tracking for a class of interconnected nonlinear systems using variable structure control, Automatica 24 (2) (1988) 187–193.
[12] V. Utkin, J. Shi, Integral sliding mode in systems operating under uncertainty conditions, in: Proceedings of 35th IEEE Conference on Decision and Control, IEEE, 1996.
[13] S.X. Ding, Integrated design of feedback controllers and fault detectors, Annu. Rev. Control 33 (2009) 124–135.
[14] L. Chen, H. Alwi, C. Edwards, On the synthesis of an integrated active LPV FTC scheme using sliding modes, Automatica 110 (2019).
[15] J. Lan, R.J. Patton, Robust Integration of Model-Based Fault Estimation and Fault-Tolerant Control, Springer International Publishing, 2020-12-11.
[16] C.T. Nett, C.A. Jacobson, A.T. Miller, An integrated approach to controls and diagnostics: The 4-parameter controller, in: Proc. Amer. Contr, Conf, 1988, pp. 824–835.
[17] A. Marcos, G.J. Balas, A robust integrated controller/diagnosis aircraft application, Internat. J. Robust Nonlinear Control 15 (12) (2005) 531–551.
[18] H. Wang, G.H. Yang, Integrated fault detection and control for LPV systems, Internat. J. Robust Nonlinear Control 19 (2009) 341–363.
[19] T. Suzuki, M. Tomizuka, Joint synthesis of fault detector and controller based on structure of two-degree-of-freedom control system, in: Proceedings of the IEEE CDC, 1999.
[20] K. Zhou, Z. Ren, A new controller architecture for high performance, robust, and fault-tolerant control, IEEE Trans. Autom. Control 46 (2001) 1613–1618.
[21] D. Henry, A. Zolghadri, Design and analysis of robust residual generators for systems under feedback control, Automatica 41 (2005) 251–264.
[22] L. Chen, H. Alwi, C. Edwards, M. Sato, Flight evaluation of an LPV sliding mode observer for sensor FTC, IEEE Trans. Control Syst. Technol. 30 (2022) 1319–1327.
[23] K. Zhou, J. Doyle, Essentials of Robust Control, Prentice Hall, 1998.
[24] V.I. Utkin, Sliding Modes in Control and Optimization, Springer, Berlin Heidelberg, 1992.
[25] L. Chen, H. Alwi, C. Edwards, M. Sato, Flight evaluation of a sliding mode online control allocation scheme for fault tolerant control, Automatica 114 (2020).
[26] H. Alwi, C. Edwards, Fault tolerant control using sliding modes with on-line control allocation, Automatica 44 (7) (2008) 1859–1866.
[27] O. Harkegard, S. Glad, Resolving actuator redundancy - optimal vs. control allocation, Automatica 41 (1) (2005) 137–144.
[28] F. Castanos, L. Fridman, Analysis and design of integral sliding manifolds for systems with unmatched perturbations, IEEE Trans. Automat. Control 51 (5) (2006) 853–858.
[29] J. Mohammadpour, C. Scherer, Control of Linear Parameter Varying Systems with Applications, Springer, 2012.
[30] D. Rotondo, F. Nejjari, V. Puig, Robust state-feedback control of uncertain LPV systems: An LMI-based approach, J. Franklin Inst. 351 (2014) 2781–2803.
[31] W.M. Haddad, D.S. Bernstein, Explicit construction of quadratic Lyapunov functions for the small gain, positivity, circle and popov theorems and their application to robust stability, Internat. J. Robust Nonlinear Control 3 (1993) 313–339.
[32] T. Khong, J.-Y. Shin, Robustness analysis of integrated LPV-FDI filters and LTI-FTC system for a transport aircraft, in: AIAA Guidance, Navigation and Control Conference and Exhibit, American Institute of Aeronautics and Astronautics, 2007.
[33] H. Alwi, C. Edwards, A. Marcos, Fault reconstruction using a LPV sliding mode observer for a class of LPV systems, J. Franklin Inst. 349 (2) (2012) 510–530.